Long-term numerical simulation of the interaction between a neutron field and a neutral meson field by a symplectic-preserving scheme

2008 J. Phys. A: Math. Theor. 41 255207

(http://iopscience.iop.org/1751-8121/41/25/255207)

IOP PUBLISHING JOURNAL OF PHYSICS A: MATHEMATICAL AND THEORETICAL

J. Phys. A: Math. Theor. **41** (2008) 255207 (19pp) doi:10.1088/1751-8113/41/25/255207

Long-term numerical simulation of the interaction between a neutron field and a neutral meson field by a symplectic-preserving scheme

Linghua Kong[1], **Jialin Hong**[2] **and Ruxun Liu**[3]

[1] School of Mathematics and Information Science, Jiangxi Normal University, Nanchang, Jiangxi 330022, People's Republic of China
[2] State Key Laboratory of Scientific and Engineering Computing, Institute of Computational Mathematics and Scientific/Engineering Computing, AMSS, CAS, PO Box 2719, Beijing 100080, People's Republic of China
[3] Department of Mathematics, University of Science and Technology of China, Hefei, Anhui 230026, People's Republic of China

E-mail: konglh@mail.ustc.edu.cn, hjl@lsec.cc.ac.cn and liurx@ustc.edu.cn

Received 1 December 2007, in final form 31 March 2008
Published 4 June 2008
Online at stacks.iop.org/JPhysA/41/255207

Abstract

In this paper, we propose a family of symplectic structure-preserving numerical methods for the coupled Klein–Gordon–Schrödinger (KGS) system. The Hamiltonian formulation is constructed for the KGS. We discretize the Hamiltonian system in space first with a family of canonical difference methods which convert an infinite-dimensional Hamiltonian system into a finite-dimensional one. Next, we discretize the finite-dimensional system in time by a midpoint rule which preserves the symplectic structure of the original system. The conservation laws of the schemes are analyzed in succession, including the charge conservation law and the residual of energy conservation law, etc. We analyze the truncation errors and global errors of the numerical solutions for the schemes to end the theoretical analysis. Extensive numerical tests show the accordance between the theoretical and numerical results.

PACS numbers: 02.60.Jh, 45.20.Jj

(Some figures in this article are in colour only in the electronic version)

1. Introduction

Rapid progress has been made in symplectic structure-preserving numerical methods for Hamiltonian ODEs since they were systematically brought forward by Feng [1] in 1984. They are more efficient than the traditional numerical schemes for long-term numerical simulations, and nowadays, are applied to a number of practical problems arising in many fields of science

and engineering, such as celestial mechanics, quantum physics, and statistical physics. See [2–9] and references therein.

In this paper, we focus on the symplectic schemes for the standard coupled Klein–Gordon–Schrödinger (KGS) system. The model describes the interaction between a conserved scalar neutron field and a neutral meson field, and plays an important role in quantum physics. In the last three decades many researchers have paid their attention to the model from the partial differential equations aspect [12–17]. Moreover, many authors have studied its exact solutions [18–20]. Nevertheless, to our knowledge, study of its numerical methods, especially numerical simulations, is extremely limited. In [21, 22], Zhang *et al* presented some energy-preserving difference schemes for it. In [23], Xiang exhibited a Fourier spectral method for it. Unfortunately, none of them performed any numerical experiment, only theoretically numerical analysis. As for numerical methods with numerical illustrations, we established multisymplectic schemes for it [24, 25], and Hong *et al* estimated the errors for the multisymplectic schemes [26], and Bao *et al* presented spectral splitting methods for it [27].

The standard coupled KGS system is the following mathematical model:

$$\begin{cases} \mathrm{i}\psi_t + \frac{1}{2}\psi_{xx} + \psi\varphi = 0, \\ \varphi_{tt} - \varphi_{xx} + \varphi - |\psi|^2 = 0, \end{cases} \qquad (x,t) \in \mathbb{R} \times \mathbb{R}^+, \tag{1}$$

where $\mathrm{i} = \sqrt{-1}$, the complex unknown function $\psi(x,t)$ represents a scalar neutron field, and the real unknown function $\varphi(x,t)$ represents a scalar neutral meson field. We consider the initial-boundary value problem for the KGS (1) by prescribing the conditions

$$\psi(x,0) = \psi_0(x), \qquad \varphi(x,0) = \varphi_0(x), \qquad \varphi_t(x,0) = \varphi_1(x), \tag{2}$$

$$\lim_{|x|\to\infty} |\psi(x,t)| = 0, \qquad \lim_{|x|\to\infty} \varphi(x,t) = 0, \tag{3}$$

where $\psi_0(x), \varphi_0(x), \varphi_1(x)$ are known smooth functions. The numerical methods which will be presented in the paper can be extended to periodic boundary problems.

The initial-boundary value problem (1)–(3) at least admits the following two invariants.

(i) The charge is conserved, that is,

$$\mathcal{A}(t) = \|\psi(x,t)\|^2 = \int_{\mathbb{R}} |\psi(x,t)|^2 \,\mathrm{d}x = \int_{\mathbb{R}} |\psi_0(x)|^2 \,\mathrm{d}x = \mathcal{A}(0). \tag{4}$$

(ii) The energy or the Hamiltonian quantity is conserved, namely,

$$\mathcal{E}(t) = \mathcal{E}(0), \tag{5}$$

where $\mathcal{E}(t) = \int_{\mathbb{R}} \left[\frac{1}{2}\left(\varphi^2(x,t) + \varphi_t^2(x,t) + \varphi_x^2(x,t) + |\psi_x(x,t)|^2\right) - |\psi(x,t)|^2\varphi(x,t)\right] \mathrm{d}x$.

Furthermore, the KGS (1) can be cast into a Hamiltonian framework. In fact, let $\psi(x,t) = p(x,t) + \mathrm{i}q(x,t)$, $\varphi_t(x,t) = 2v(x,t)$, where $p(x,t), q(x,t)$ are real functions, then we get the infinite-dimensional Hamiltonian formulation

$$\frac{\mathrm{d}}{\mathrm{d}t} z = J \frac{\delta H(z)}{\delta z}, \tag{6}$$

where $z = [q, v, p, \varphi]^T$, $J = \begin{bmatrix} \mathbf{0} & J_1 \\ -J_1 & \mathbf{0} \end{bmatrix}$, $J_1 = \begin{bmatrix} \frac{1}{2} & 0 \\ 0 & 1 \end{bmatrix}$. The Hamiltonian function is

$$H(z) = \int_{\mathbb{R}} \left[\varphi(p^2 + q^2) - \frac{1}{2}\left(\varphi^2 + \varphi_x^2 + p_x^2 + q_x^2\right) - v^2\right] \mathrm{d}x.$$

The paper is organized as follows. In section 2, we establish a family of symplectic approximations for the KGS (1) which is discretized by the canonical difference method in the spatial direction and the Euler midpoint rule in the temporal direction. It is discovered that the schemes are charge preserving. Furthermore, the residual of energy is also analyzed in the section. In section 3, we focus our discussion on the error analysis of the numerical solutions of the schemes we construct, and prove that they converge to the exact solutions with second-order accuracy in time and $2m$th order in space. In section 4, we test the accuracy and invariants of our methods for the KGS with solitary wave solution. The schemes are also applied to simulate plane wave and various solitons of the KGS. Finally, some conclusions are summarized from the theoretical discussion and numerical results.

2. Symplectic approximation for the KGS

We consider the determined problem (1)–(3) in the temporal-spatial domain $[-L, L] \times [0, T] \subset \mathbb{R} \times \mathbb{R}^+$ and divide the domain into a uniform mesh $\{(x_j, t_n) \mid x_j = -L + jh, t_n = n\tau, j = 0, 1, 2, \ldots, N; n = 0, 1, 2, \ldots, M\}$, where $h = \frac{2L}{N}$ is the spatial mesh step size and $\tau = \frac{T}{M}$ is the temporal step length. The approximation of the function $u(x, t)$ at the mesh point (x_j, t_n) is denoted by u_j^n. Furthermore, the following notations are employed:

$$u_j^{n+\frac{1}{2}} = \frac{1}{2}\left(u_j^n + u_j^{n+1}\right), \qquad \delta_t u_j^{n+\frac{1}{2}} = \frac{u_j^{n+1} - u_j^n}{\tau},$$

and

$$\langle u^n, v^n \rangle = h \sum_j u_j^n \overline{v_j^n}, \qquad \|u^n\|^2 = h \sum_j u_j^n \overline{u_j^n}, \qquad \|u^n\|_\infty = \max_{0 \leqslant j \leqslant N} \left|u_j^n\right|,$$

where $\overline{u_j^n}$ is the complex conjugate of u_j^n. For simplicity, we have written the sum $\sum_{j=0}^N$ as $\sum_j$ in the last two sum.

To convert an infinite-dimensional Hamiltonian system (6) into a finite-dimensional one, we first discretize it in the spatial direction. Approximating the second-order partial derivative operator $\frac{\partial^2}{\partial x^2}$ by $\mathcal{B}(2m)$ [3] at the nodes x_j, it yields

$$\mathcal{B}(2m) = \nabla_+ \nabla_- \sum_{j=0}^{m-1} (-1)^j \beta_j \left(\frac{h^2 \nabla_+ \nabla_-}{4}\right)^j, \tag{7}$$

where $\beta_j = \frac{(j!)^2 4^j}{(2j+1)!(j+1)}$, and ∇_+, ∇_- are the forward and backward difference quotient operators, respectively. It is easy to verify that $\beta_0 = 1, \beta_1 = \frac{1}{3}, \beta_2 = \frac{8}{45}$. Therefore, the differential matrices corresponding to $\frac{\partial^2}{\partial x^2}$ for homogeneous condition, for $m = 1, 2, 3$, are $(N-1) \times (N-1)$ symmetric Toeplitz matrices whose first rows are given by

$$\frac{1}{h^2}[-2, 1, 0, \ldots, 0], \qquad \frac{1}{12h^2}[-30, 16, -1, 0, \ldots, 0],$$
$$\frac{1}{180h^2}[-490, 270, -27, 2, 0, \ldots, 0],$$

respectively. These matrices for $m = 1, 2, 3$ are denoted by B_2, B_4, B_6, respectively.

Remark 1. The above matrices are suitable for the homogeneous boundary conditions. As for the periodic boundary conditions, these matrices ought to be $N \times N$ circulant matrices,

whose first rows for $m = 1, 2, 3$, are

$$\frac{1}{h^2}[-2, 1, 0, \ldots, 0, 1],$$
$$\frac{1}{12h^2}[-30, 16, -1, 0, \ldots, 0, -1, 16],$$
$$\frac{1}{180h^2}[-490, 270, -27, 2, 0, \ldots, 0, 2, -27, 270],$$

respectively. We still denote these matrices as B_2, B_4, B_6.

From the positive definiteness of $-B_{2m}$, there exists a matrix G_{2m}, such that

$$-B_{2m} = G_{2m}^T G_{2m}.$$

Replacing $\frac{\partial^2}{\partial x^2}$ in the infinite-dimensional Hamiltonian system (6) by $\mathcal{B}(2m)$, we obtain a semi-discrete system whose accuracy in space is $O(h^{2m})$,

$$\begin{bmatrix} Q_t \\ V_t \\ P_t \\ \Phi_t \end{bmatrix} = \begin{bmatrix} 0 & 0 & I_N & 0 \\ 0 & 0 & 0 & I_N \\ -I_N & 0 & 0 & 0 \\ 0 & -I_N & 0 & 0 \end{bmatrix} \begin{bmatrix} M_1 & 0 & 0 & 0 \\ 0 & M_2 & 0 & 0 \\ 0 & 0 & M_3 & 0 \\ 0 & 0 & 0 & M_4 \end{bmatrix} \begin{bmatrix} Q \\ V \\ P \\ \Phi \end{bmatrix}, \tag{8}$$

where I_N is the $N \times N$ identity matrix, $M_1 = \frac{1}{2}B_{2m} + D_1$, $M_2 = -2I_N$, $M_3 = \frac{1}{2}B_{2m} + D_3$, $M_4 = \frac{1}{2}(B_{2m} - I_N) + D_4$, with the diagonal matrices

$$D_1 = D_3 = \operatorname{diag}(\varphi_1, \varphi_2, \ldots, \varphi_N),\ D_4 = \frac{1}{2}\operatorname{diag}\left(\frac{p_1^2 + q_1^2}{\varphi_1}, \frac{p_2^2 + q_2^2}{\varphi_2}, \ldots, \frac{p_N^2 + q_N^2}{\varphi_N}\right).$$

And $Z = [Q^T, V^T, P^T, \Phi^T]^T$, $Q = [q_1(t), q_2(t), \ldots, q_N(t)]^T$, $P = [p_1(t), p_2(t), \ldots, p_N(t)]^T$, $V = [v_1(t), v_2(t), \ldots, v_N(t)]^T$, $\Phi = [\varphi_1(t), \varphi_2(t), \ldots, \varphi_N(t)]^T$.

The semi-discretization (8) is a finite-dimensional Hamiltonian system because B_{2m} is symmetric [10], whose Hamiltonian function is

$$H(Z) = \frac{1}{4}(P^T B_{2m} P + Q^T B_{2m} Q) + \frac{1}{4}\Phi^T (B_{2m} - I_N)\Phi + V^T V + \frac{1}{2}\sum_{j=1}^{N} \varphi_j \left(p_j^2 + q_j^2\right).$$

We discretize (8) in time further with the midpoint rule and arrive at a symplectic integrator

$$\frac{Q^{n+1} - Q^n}{\tau} = \frac{1}{2}B_{2m} P^{n+\frac{1}{2}} + \Phi^{n+\frac{1}{2}} \cdot P^{n+\frac{1}{2}}, \tag{9}$$

$$\frac{V^{n+1} - V^n}{\tau} = \frac{1}{2}(B_{2m} - I_N)\Phi^{n+\frac{1}{2}} + \frac{1}{2}\Phi^{n+\frac{1}{2}} \cdot \left[\left(P^{n+\frac{1}{2}}\right) \cdot^2 + \left(Q^{n+\frac{1}{2}}\right) \cdot^2\right], \tag{10}$$

$$\frac{P^{n+1} - P^n}{\tau} = -\left[\frac{1}{2}B_{2m} Q^{n+\frac{1}{2}} + \Phi^{n+\frac{1}{2}} \cdot Q^{n+\frac{1}{2}}\right], \tag{11}$$

$$\frac{\Phi^{n+1} - \Phi^n}{\tau} = 2V^{n+\frac{1}{2}}, \tag{12}$$

where '$\cdot$' is the componentwise product between vectors, $P \cdot Q = [p_1 q_1, p_2 q_2, \ldots, p_N q_N]^T$, for example.

It follows from (9)–(12) that

$$\mathrm{i}\frac{\Psi^{n+1} - \Psi^n}{\tau} + \frac{1}{2}B_{2m}\Psi^{n+\frac{1}{2}} = -\Phi^{n+\frac{1}{2}} \cdot \Psi^{n+\frac{1}{2}}, \tag{13}$$

$$\frac{\Phi^{n+1} - 2\Phi^n + \Phi^{n-1}}{\tau^2} - \frac{1}{2}(B_{2m} - I_N)\left(\Phi^{n+\frac{1}{2}} + \Phi^{n-\frac{1}{2}}\right) = \frac{1}{2}\left(\left|\Psi^{n+\frac{1}{2}}\right| \cdot^2 + \left|\Psi^{n-\frac{1}{2}}\right| \cdot^2\right), \tag{14}$$

where $\Psi^n = P^n + \mathrm{i}Q^n = \left(p_1^n, p_2^n, \ldots, p_N^n\right)^T + \mathrm{i}\left(q_1^n, q_2^n, \ldots, q_N^n\right)^T = \left(\psi_1^n, \psi_2^n, \ldots, \psi_N^n\right)^T$, etc.

Theorem 1. *The symplectic scheme (13)–(14) conserves the charge exactly, i.e.,*

$$\mathcal{A}^{n+1} = \|\Psi^{n+1}\|^2 = h\sum_j \left|\psi_j^{n+1}\right|^2 = h\sum_j \left|\psi_{0j}\right|^2 = \|\Psi^0\|^2 = \mathcal{A}^0. \tag{15}$$

Thus the scheme is stable with respect to the initial value.

Proof. Taking the complex inner product of (13) with $\Psi^{n+\frac{1}{2}}$, we have

$$\frac{\mathrm{i}}{2\tau}\langle\Psi^{n+1} - \Psi^n, \Psi^{n+1} + \Psi^n\rangle + \frac{1}{2}\left\langle B_{2m}\Psi^{n+\frac{1}{2}}, \Psi^{n+\frac{1}{2}}\right\rangle + \left\langle\Phi^{n+\frac{1}{2}}\cdot\Psi^{n+\frac{1}{2}}, \Psi^{n+\frac{1}{2}}\right\rangle = 0. \tag{16}$$

The second term in the left side of equality (16) is real because of the symmetry of B_{2m}, and the third term is also real. The rest is

$$\frac{\mathrm{i}}{2\tau}(\|\Psi^{n+1}\|^2 - \|\Psi^n\|^2 + \langle\Psi^{n+1}, \Psi^n\rangle - \langle\Psi^n, \Psi^{n+1}\rangle) = \frac{\mathrm{i}}{2\tau}(\mathcal{A}^{n+1} - \mathcal{A}^n) - \frac{1}{\tau}\mathrm{Im}\langle\Psi^{n+1}, \Psi^n\rangle,$$

where 'Im' stands for the imaginary part.

Therefore, the imaginary part of (16) is

$$\frac{\mathrm{i}}{2\tau}(\mathcal{A}^{n+1} - \mathcal{A}^n) = 0, \tag{17}$$

which means

$$\mathcal{A}^{n+1} = \mathcal{A}^n.$$

We can get the conclusion (15) by induction. This completes the proof. □

Remark 2. We have applied the homogeneous boundary conditions (3) to prove the above theorem. The conclusions to which we arrive are also true for periodic boundary conditions and can be proved almost in the same way.

It is obvious that theorem 1 is a discrete version of the charge conservation law (4), as a quadratic invariant, which plays a very important role in quantum physics.

The symplectic approximation (13)–(14) cannot conserve the total energy (5) exactly because of the nonlinearity of the KGS (1). The following result provides the energy residual.

Theorem 2. *The total residual of energy of the symplectic approximation (13)–(14) is*

$$\mathrm{Res}^{n+\frac{1}{2}} = \frac{\mathcal{E}^{n+\frac{1}{2}} - \mathcal{E}^{n-\frac{1}{2}}}{\tau} = \frac{1}{\tau}h\sum_j \left|\psi_j^{n+\frac{1}{2}} - \psi_j^{n-\frac{1}{2}}\right|^2\left(\varphi_j^{n+\frac{1}{2}} - \varphi_j^{n-\frac{1}{2}}\right), \tag{18}$$

where $\mathcal{E}^{n+\frac{1}{2}} = \left\|\delta_t\Phi^{n+\frac{1}{2}}\right\|^2 + \left\|\Phi^{n+\frac{1}{2}}\right\|^2 + \left\|G_{2m}\Phi^{n+\frac{1}{2}}\right\|^2 + \left\|G_{2m}\Psi^{n+\frac{1}{2}}\right\|^2 - 2h\sum_j \varphi_j^{n+\frac{1}{2}}\left|\psi_j^{n+\frac{1}{2}}\right|^2$, *which is a discrete version of energy expression defined in (5).*

Proof. The equality (13) can be written as

$$\mathrm{i}\left(\delta_t\Psi^{n+\frac{1}{2}} + \delta_t\Psi^{n-\frac{1}{2}}\right) + \frac{1}{2}B_{2m}\left(\Psi^{n+\frac{1}{2}} + \Psi^{n-\frac{1}{2}}\right) + \left(\Phi^{n+\frac{1}{2}}\cdot\Psi^{n+\frac{1}{2}} + \Phi^{n-\frac{1}{2}}\cdot\Psi^{n-\frac{1}{2}}\right) = 0. \tag{19}$$

Computing the inner product of (19) with $\delta_t\Psi^{n+\frac{1}{2}}+\delta_t\Psi^{n-\frac{1}{2}}=\frac{\Psi^{n+1}-\Psi^{n-1}}{\tau}=\frac{2}{\tau}\big(\Psi^{n+\frac{1}{2}}-\Psi^{n-\frac{1}{2}}\big)$, we have

$$\begin{aligned}
&\frac{\mathrm{i}}{\tau^2}\|\Psi^{n+1}-\Psi^{n-1}\|^2+\frac{1}{\tau}\big\langle B_{2m}\big(\Psi^{n+\frac{1}{2}}+\Psi^{n-\frac{1}{2}}\big),\Psi^{n+\frac{1}{2}}-\Psi^{n-\frac{1}{2}}\big\rangle\\
&\qquad+\frac{2}{\tau}\big\langle\Phi^{n+\frac{1}{2}}\cdot\Psi^{n+\frac{1}{2}}+\Phi^{n-\frac{1}{2}}\cdot\Psi^{n-\frac{1}{2}},\Psi^{n+\frac{1}{2}}-\Psi^{n-\frac{1}{2}}\big\rangle\\
&\qquad=\frac{\mathrm{i}}{\tau^2}\|\Psi^{n+1}-\Psi^{n-1}\|^2+\frac{1}{\tau}\big[\big\langle B_{2m}\Psi^{n+\frac{1}{2}},\Psi^{n+\frac{1}{2}}\big\rangle-\big\langle B_{2m}\Psi^{n-\frac{1}{2}},\Psi^{n-\frac{1}{2}}\big\rangle\big]\\
&\qquad+\frac{2}{\tau}h\sum_j\big(\varphi_j^{n+\frac{1}{2}}\big|\psi_j^{n+\frac{1}{2}}\big|^2-\varphi_j^{n-\frac{1}{2}}\big|\psi_j^{n-\frac{1}{2}}\big|^2\big)\\
&\qquad+\frac{2}{\tau}h\sum_j\big(\varphi_j^{n-\frac{1}{2}}\psi_j^{n-\frac{1}{2}}\overline{\psi_j^{n+\frac{1}{2}}}-\varphi_j^{n+\frac{1}{2}}\psi_j^{n+\frac{1}{2}}\overline{\psi_j^{n-\frac{1}{2}}}\big)\\
&\qquad=0.
\end{aligned}$$

The first and the second terms of the above equality are pure imaginary and real functions, respectively. Therefore, its real part is

$$\begin{aligned}
&\frac{1}{\tau}\left[\left(\big\|G_{2m}\Psi^{n+\frac{1}{2}}\big\|^2+2h\sum_j\varphi_j^{n+\frac{1}{2}}\big|\psi_j^{n+\frac{1}{2}}\big|^2\right)-\left(\big\|G_{2m}\Psi^{n-\frac{1}{2}}\big\|^2+2h\sum_j\varphi_j^{n-\frac{1}{2}}\big|\psi_j^{n-\frac{1}{2}}\big|^2\right)\right]\\
&\qquad=-\frac{2}{\tau}\mathcal{R}\left\{h\sum_j\big(\varphi_j^{n-\frac{1}{2}}\psi_j^{n-\frac{1}{2}}\overline{\psi_j^{n+\frac{1}{2}}}-\varphi_j^{n+\frac{1}{2}}\psi_j^{n+\frac{1}{2}}\overline{\psi_j^{n-\frac{1}{2}}}\big)\right\},
\end{aligned}\tag{20}$$

where '$\mathcal{R}$' stands for the real part. Recall that we have employed the fact

$$\big\langle B_{2m}\Psi^{n+\frac{1}{2}},\Psi^{n+\frac{1}{2}}\big\rangle=\big\|G_{2m}\Psi^{n+\frac{1}{2}}\big\|^2.$$

Let $B_{2m}-I_N=A_{2m}$, then A_{2m} is symmetric for the symmetry of B_{2m} and I_N.

Taking the inner product of (14) with $\delta_t\Phi^{n+\frac{1}{2}}+\delta_t\Phi^{n-\frac{1}{2}}=\frac{\Phi^{n+1}-\Phi^{n-1}}{\tau}=\frac{2}{\tau}\big(\Phi^{n+\frac{1}{2}}-\Phi^{n-\frac{1}{2}}\big)$, it yields

$$\begin{aligned}
&\frac{1}{\tau}\left\{\big\langle\delta_t\Phi^{n+\frac{1}{2}}-\delta_t\Phi^{n-\frac{1}{2}},\delta_t\Phi^{n+\frac{1}{2}}+\delta_t\Phi^{n-\frac{1}{2}}\big\rangle-\big\langle A_{2m}\big(\Phi^{n+\frac{1}{2}}+\Phi^{n-\frac{1}{2}}\big),\Phi^{n+\frac{1}{2}}-\Phi^{n-\frac{1}{2}}\big\rangle\right.\\
&\qquad\left.-h\sum_j\big(\big|\psi_j^{n+\frac{1}{2}}\big|^2+\big|\psi_j^{n-\frac{1}{2}}\big|^2\big)\big(\varphi_j^{n+\frac{1}{2}}-\varphi_j^{n-\frac{1}{2}}\big)\right\}\\
&\qquad=\frac{1}{\tau}\left\{\big(\big\|\delta_t\Phi^{n+\frac{1}{2}}\big\|^2+\big\langle-A_{2m}\Phi^{n+\frac{1}{2}},\Phi^{n+\frac{1}{2}}\big\rangle\big)-\big(\big\|\delta_t\Phi^{n-\frac{1}{2}}\big\|^2+\big\langle-A_{2m}\Phi^{n-\frac{1}{2}},\Phi^{n-\frac{1}{2}}\big\rangle\big)\right.\\
&\qquad\left.-h\sum_j\big(\big|\psi_j^{n+\frac{1}{2}}\big|^2+\big|\psi_j^{n-\frac{1}{2}}\big|^2\big)\big(\varphi_j^{n+\frac{1}{2}}-\varphi_j^{n-\frac{1}{2}}\big)\right\}\\
&\qquad=0.
\end{aligned}$$

With $-A_{2m}=I_N-B_{2m}$, it derives that $\big\langle-A_{2m}\Phi^{n+\frac{1}{2}},\Phi^{n+\frac{1}{2}}\big\rangle=\big\|G_{2m}\Phi^{n+\frac{1}{2}}\big\|^2+\big\|\Phi^{n+\frac{1}{2}}\big\|^2$ and $\big\langle-A_{2m}\Phi^{n-\frac{1}{2}},\Phi^{n-\frac{1}{2}}\big\rangle=\big\|G_{2m}\Phi^{n-\frac{1}{2}}\big\|^2+\big\|\Phi^{n-\frac{1}{2}}\big\|^2$. From the above analysis, we can further deduce

$$\begin{aligned}
&\frac{1}{\tau}\big\{\big(\big\|\delta_t\Phi^{n+\frac{1}{2}}\big\|^2+\big\|\Phi^{n+\frac{1}{2}}\big\|^2+\big\|G_{2m}\Phi^{n+\frac{1}{2}}\big\|^2\big)-\big(\big\|\delta_t\Phi^{n-\frac{1}{2}}\big\|^2+\big\|\Phi^{n-\frac{1}{2}}\big\|^2+\big\|G_{2m}\Phi^{n-\frac{1}{2}}\big\|^2\big)\big\}\\
&\qquad=\frac{1}{\tau}h\sum_j\big(\big|\psi_j^{n+\frac{1}{2}}\big|^2+\big|\psi_j^{n-\frac{1}{2}}\big|^2\big)\big(\varphi_j^{n+\frac{1}{2}}-\varphi_j^{n-\frac{1}{2}}\big).
\end{aligned}\tag{21}$$

It follows that (20) and (21) yield

$$\begin{aligned}\frac{\mathcal{E}^{n+\frac{1}{2}}-\mathcal{E}^{n-\frac{1}{2}}}{\tau} &= \frac{1}{\tau}h\sum_j\Big\{\big(|\psi_j^{n+\frac{1}{2}}|^2+|\psi_j^{n-\frac{1}{2}}|^2\big)\big(\varphi_j^{n+\frac{1}{2}}-\varphi_j^{n-\frac{1}{2}}\big)\\ &\quad+2\mathcal{R}\big(\varphi_j^{n-\frac{1}{2}}\psi_j^{n-\frac{1}{2}}\overline{\psi_j^{n+\frac{1}{2}}}-\varphi_j^{n+\frac{1}{2}}\psi_j^{n+\frac{1}{2}}\overline{\psi_j^{n-\frac{1}{2}}}\big)\Big\}\\ &= \frac{1}{\tau}h\sum_j\Big\{\big(|\psi_j^{n+\frac{1}{2}}|^2+|\psi_j^{n-\frac{1}{2}}|^2\big)\big(\varphi_j^{n+\frac{1}{2}}-\varphi_j^{n-\frac{1}{2}}\big)+\big(\varphi_j^{n-\frac{1}{2}}\psi_j^{n-\frac{1}{2}}\overline{\psi_j^{n+\frac{1}{2}}}\\ &\quad-\varphi_j^{n+\frac{1}{2}}\psi_j^{n+\frac{1}{2}}\overline{\psi_j^{n-\frac{1}{2}}}+\varphi_j^{n-\frac{1}{2}}\overline{\psi_j^{n-\frac{1}{2}}}\psi_j^{n+\frac{1}{2}}-\varphi_j^{n+\frac{1}{2}}\overline{\psi_j^{n+\frac{1}{2}}}\psi_j^{n-\frac{1}{2}}\big)\Big\}\\ &= \frac{1}{\tau}h\sum_j\Big\{\big(\psi_j^{n+\frac{1}{2}}\overline{\psi_j^{n+\frac{1}{2}}}+\psi_j^{n-\frac{1}{2}}\overline{\psi_j^{n-\frac{1}{2}}}\big)\big(\varphi_j^{n+\frac{1}{2}}-\varphi_j^{n-\frac{1}{2}}\big)\\ &\quad-\big(\psi_j^{n-\frac{1}{2}}\overline{\psi_j^{n+\frac{1}{2}}}+\psi_j^{n+\frac{1}{2}}\overline{\psi_j^{n-\frac{1}{2}}}\big)\big(\varphi_j^{n+\frac{1}{2}}-\varphi_j^{n-\frac{1}{2}}\big)\Big\}\\ &= \frac{1}{\tau}h\sum_j|\psi_j^{n+\frac{1}{2}}-\psi_j^{n-\frac{1}{2}}|^2\big(\varphi_j^{n+\frac{1}{2}}-\varphi_j^{n-\frac{1}{2}}\big).\end{aligned}$$

This finishes the proof. □

3. Error estimations for the symplectic approximation

In what follows, we further discuss the numerical properties of the symplectic scheme (13)–(14), including its convergence, truncation errors and stability, etc. These properties are the most important signs for a numerical method.

We denote the truncation errors of the symplectic approximation (13)–(14) by

$$R^n=\mathrm{i}\delta_t\Psi\big(\cdot,t_{n+\frac{1}{2}}\big)+\tfrac{1}{2}B_{2m}\Psi\big(\cdot,t_{n+\frac{1}{2}}\big)+\Phi\big(\cdot,t_{n+\frac{1}{2}}\big)\cdot\Psi\big(\cdot,t_{n+\frac{1}{2}}\big), \tag{22}$$

$$\begin{aligned}S^n&=\delta_t^2\Phi(\cdot,t_n)-\tfrac{1}{2}(B_{2m}-I_N)\big(\Phi\big(\cdot,t_{n+\frac{1}{2}}\big)+\Phi\big(\cdot,t_{n-\frac{1}{2}}\big)\big)\\ &\quad-\tfrac{1}{2}\big(\big|\Psi\big(\cdot,t_{n+\frac{1}{2}}\big)\big|\cdot^2+\big|\Psi\big(\cdot,t_{n-\frac{1}{2}}\big)\big|\cdot^2\big),\end{aligned} \tag{23}$$

where $\Psi(\cdot,t_n)=(\psi(x_1,t_n),\psi(x_2,t_n),\ldots,\psi(x_N,t_n))^T$, etc.

We can easily get the following truncation error by Taylor expansion.

Theorem 3. *The truncation errors of the symplectic scheme (13)–(14) is* $\mathcal{O}(\tau^2+h^{2m})$.

C is a general non-negative constant in the following. Note that it may be different at different places.

Assume that the global errors of the numerical solutions ψ_j^n,φ_j^n at (x_j,t_n) are

$$e_j^n=\psi(x_j,t_n)-\psi_j^n,\qquad \Upsilon_j^n=\varphi(x_j,t_n)-\varphi_j^n,$$

then we have the following error estimating lemma.

Lemma 1. *The symplectic scheme (13)–(14) satisfies the error estimation*

$$\max\big\{\|e^M\|^2,\big\|\Upsilon^{M+\frac{1}{2}}\big\|^2,\big\|\delta_t\Upsilon^{M+\frac{1}{2}}\big\|^2,\big\|G_{2m}\Upsilon^{M+\frac{1}{2}}\big\|^2\big\}\leqslant\left(W^0+\tau\sum_{k=1}^{M}A^k\right)e^{4CM\tau}, \tag{24}$$

provided that τ *is sufficiently small, such that* $\tau<\frac{1}{4C}$, *where* $W^n=\|e^{n+1}\|^2+\|e^n\|^2+\big\|\Upsilon^{n+\frac{1}{2}}\big\|^2+\big\|\delta_t\Upsilon^{n+\frac{1}{2}}\big\|^2+\big\|G_{2m}\Upsilon^{n+\frac{1}{2}}\big\|^2$, $A^k=\|R^k\|^2+\|R^{k-1}\|^2+\|S^k\|^2$.

Proof. It is true from theorem 1 that

$$\left|\psi_j^n\right| \leqslant C, \qquad \text{for any} \quad j, n.$$

Furthermore, for the bounded solutions of the KGS (1), we have

$$|\psi(x_j, t_n)| \leqslant C, \qquad \text{for any} \quad j, n.$$

Subtracting (13) from (22), it yields

$$R^n = \mathrm{i}\delta_t e^{n+\frac{1}{2}} + \tfrac{1}{2}B_{2m}e^{n+\frac{1}{2}} + \Phi\big(\cdot, t_{n+\frac{1}{2}}\big)\cdot\Psi\big(\cdot, t_{n+\frac{1}{2}}\big) - \Phi^{n+\frac{1}{2}}\cdot\Psi^{n+\frac{1}{2}}. \tag{25}$$

Taking the inner product of (25) with $2e^{n+\frac{1}{2}}$ and taking the imaginary part, one has

$$\begin{aligned}\frac{1}{\tau}(\|e^{n+1}\|^2 - \|e^n\|^2) &= 2\mathcal{I}\big\langle R^n, e^{n+\frac{1}{2}}\big\rangle - 2\mathcal{I}\big\langle\Psi\big(\cdot, t_{n+\frac{1}{2}}\big)\cdot\Upsilon^{n+\frac{1}{2}}, e^{n+\frac{1}{2}}\big\rangle\\ &\leqslant \|R^n\|^2 + \big\|e^{n+\frac{1}{2}}\big\|^2 + C\big\|e^{n+\frac{1}{2}}\big\|^2 + C\big\|\Upsilon^{n+\frac{1}{2}}\big\|^2\\ &\leqslant \|R^n\|^2 + \frac{1}{2}(1+C)(\|e^{n+1}\|^2 + \|e^n\|^2) + C\big\|\Upsilon^{n+\frac{1}{2}}\big\|^2. \end{aligned}\tag{26}$$

On the other hand, subtracting (14) from (23), one derives

$$\begin{aligned}S^n = \frac{1}{\tau}\big(\delta_t\Upsilon^{n+\frac{1}{2}} - \delta_t\Upsilon^{n-\frac{1}{2}}\big) - \frac{1}{2}B_{2m}\big(\Upsilon^{n+\frac{1}{2}} + \Upsilon^{n-\frac{1}{2}}\big) + \frac{1}{2}\big(\Upsilon^{n+\frac{1}{2}} + \Upsilon^{n-\frac{1}{2}}\big)\\ -\frac{1}{2}\big(\big|\Psi\big(\cdot, t_{n+\frac{1}{2}}\big)\big|\,.^2 + \big|\Psi\big(\cdot, t_{n-\frac{1}{2}}\big)\big|\,.^2 - \big|\Psi^{n+\frac{1}{2}}\big|\,.^2 - \big|\Psi^{n-\frac{1}{2}}\big|\,.^2\big).\end{aligned}$$

Taking the inner product of the above equality with $\delta_t\Upsilon^{n+\frac{1}{2}} + \delta_t\Upsilon^{n-\frac{1}{2}}$, we have

$$\begin{aligned}&\frac{1}{\tau}\big[\big(\big\|\delta_t\Upsilon^{n+\frac{1}{2}}\big\|^2 + \big\|\Upsilon^{n+\frac{1}{2}}\big\|^2 + \big\|G_{2m}\Upsilon^{n+\frac{1}{2}}\big\|^2\big) - \big(\big\|\delta_t\Upsilon^{n-\frac{1}{2}}\big\|^2 + \big\|\Upsilon^{n-\frac{1}{2}}\big\|^2 + \big\|G_{2m}\Upsilon^{n-\frac{1}{2}}\big\|^2\big)\big]\\ &\quad= \big\langle S^n, \delta_t\Upsilon^{n+\frac{1}{2}} + \delta_t\Upsilon^{n-\frac{1}{2}}\big\rangle + \frac{1}{2}\big\langle\big|\Psi\big(\cdot, t_{n+\frac{1}{2}}\big)\big|\,.^2 + \big|\Psi\big(\cdot, t_{n-\frac{1}{2}}\big)\big|\,.^2\\ &\qquad - \big|\Psi^{n+\frac{1}{2}}\big|\,.^2 - \big|\Psi^{n-\frac{1}{2}}\big|.^2, \delta_t\Upsilon^{n+\frac{1}{2}} + \delta_t\Upsilon^{n-\frac{1}{2}}\big\rangle.\end{aligned}\tag{27}$$

Using Young's Inequality $ab \leqslant \frac{1}{4}a^2 + b^2 \leqslant \frac{1}{2}a^2 + b^2$, we have

$$\big\langle S^n, \delta_t\Upsilon^{n+\frac{1}{2}} + \delta_t\Upsilon^{n-\frac{1}{2}}\big\rangle \leqslant \|S^n\|^2 + \big\|\delta_t\Upsilon^{n+\frac{1}{2}}\big\|^2 + \big\|\delta_t\Upsilon^{n-\frac{1}{2}}\big\|^2. \tag{28}$$

Moreover, it derives that

$$\begin{aligned}&\frac{1}{2}\big\langle\big|\Psi\big(\cdot, t_{n+\frac{1}{2}}\big)\big|\,.^2 + \big|\Psi\big(\cdot, t_{n-\frac{1}{2}}\big)\big|\,.^2 - \big|\Psi^{n+\frac{1}{2}}\big|\,.^2 - \big|\Psi^{n-\frac{1}{2}}\big|.^2, \delta_t\Upsilon^{n+\frac{1}{2}} + \delta_t\Upsilon^{n-\frac{1}{2}}\big\rangle\\ &\quad= \frac{1}{2}\big\langle\overline{\Psi\big(\cdot, t_{n+\frac{1}{2}}\big)}e^{n+\frac{1}{2}} + \overline{\Psi\big(\cdot, t_{n-\frac{1}{2}}\big)}e^{n-\frac{1}{2}} + \Psi^{n+\frac{1}{2}}\overline{e^{n+\frac{1}{2}}}\\ &\qquad + \Psi^{n-\frac{1}{2}}\overline{e^{n-\frac{1}{2}}}, \delta_t\Upsilon^{n+\frac{1}{2}x} + \delta_t\Upsilon^{n-\frac{1}{2}}\big\rangle\\ &\quad\leqslant C\big(\big\|\delta_t\Upsilon^{n+\frac{1}{2}}\big\|^2 + \big\|\delta_t\Upsilon^{n-\frac{1}{2}}\big\|^2\big) + \frac{1}{2}C(\|e^{n+1}\|^2 + 2\|e^n\|^2 + \|e^{n-1}\|^2).\end{aligned}\tag{29}$$

It yields from (26) to (29) that

$$\begin{aligned}\frac{1}{\tau}(W^n - W^{n-1}) &\leqslant \|R^n\|^2 + \|R^{n-1}\|^2 + \|S^n\|^2 + C\big(\big\|\Upsilon^{n+\frac{1}{2}}\big\|^2 + \big\|\Upsilon^{n-\frac{1}{2}}\big\|^2\big)\\ &\quad + (1+C)\big(\big\|\delta_t\Upsilon^{n+\frac{1}{2}}\big\|^2 + \big\|\delta_t\Upsilon^{n-\frac{1}{2}}\big\|^2\big) + \frac{1+3C}{4}(\|e^{n+1}\|^2 + 2\|e^n\|^2 + \|e^{n-1}\|^2)\\ &\leqslant \|R^n\|^2 + \|R^{n-1}\|^2 + \|S^n\|^2 + C\big(\big\|\delta_t\Upsilon^{n+\frac{1}{2}}\big\|^2 + \big\|\delta_t\Upsilon^{n-\frac{1}{2}}\big\|^2\\ &\quad + \big\|\Upsilon^{n+\frac{1}{2}}\big\|^2 + \big\|\Upsilon^{n-\frac{1}{2}}\big\|^2 + \|e^{n+1}\|^2 + 2\|e^n\|^2 + \|e^{n-1}\|^2\big)\\ &\leqslant A^n + C(W^n + W^{n-1}).\end{aligned}$$

Hence, it draws from discrete Gronwall inequality [28] and the above inequality that

$$W^M \leqslant \left(W^0 + \tau \sum_{k=1}^{M} A_k \right) e^{4CM\tau}, \tag{30}$$

holds, where τ is sufficiently small, such that $\tau < \frac{1}{4C}$.

The estimation (24) holds recalling the definition of W^n. The proof is completed. □

We would like to note that the estimates are bounded by the initial values and truncation errors of the numerical methods.

Theorem 4. *The global numerical errors of the symplectic approximation (13)–(14) of KGS satisfies*

$$\|e^M\| \leqslant \mathcal{O}(\tau^2 + h^{2m}), \qquad \|\Upsilon^M\|_\infty \leqslant \mathcal{O}(\tau^2 + h^{2m}). \tag{31}$$

Proof. From

$$\|e^0\|^2 = \|\Upsilon^0\|^2 = 0, \qquad \|e^1\|^2 = \mathcal{O}(\tau^2 + h^{2m})^2, \qquad \|\Upsilon^1\|^2 = \mathcal{O}(\tau^2 + h^{2m})^2,$$
$$\|R^n\|^2 \leqslant \mathcal{O}(\tau^2 + h^{2m})^2, \qquad \|S^n\|^2 \leqslant \mathcal{O}(\tau^2 + h^{2m})^2,$$

we have

$$W^0 = \mathcal{O}(\tau^2 + h^{2m})^2.$$

It draws from theorem 3 that

$A^k = \mathcal{O}(\tau^2 + h^{2m})^2$.

Therefore,

$$\begin{aligned} W^M &= \|e^M\|^2 + \|e^{M-1}\|^2 + \left\|\Upsilon^{M-\frac{1}{2}}\right\|^2 + \left\|\delta_t \Upsilon^{M-\frac{1}{2}}\right\|^2 + \left\|G_{2m}\Upsilon^{M-\frac{1}{2}}\right\|^2 \\ &\leqslant C\mathcal{O}(\tau^2 + h^{2m})^2. \end{aligned}$$

Moreover, it follows from lemma 1 that

$$\|e^M\| \leqslant \mathcal{O}(\tau^2 + h^{2m}), \qquad \left\|\Upsilon^{M-\frac{1}{2}}\right\| \leqslant \mathcal{O}(\tau^2 + h^{2m}), \qquad \left\|G_{2m}\Upsilon^{M-\frac{1}{2}}\right\| \leqslant \mathcal{O}(\tau^2 + h^{2m}).$$

From the discrete Sobolev inequality, one discovers that

$$\|\Upsilon^M\|_\infty \leqslant \mathcal{O}(\tau^2 + h^{2m}).$$

This completes the proof. □

Similarly, we can prove that the symplectic approximation (13)–(14) is stable.

4. Numerical experiments

To illustrate the numerical performance of the symplectic approximation (13)–(14), we present some numerical experiments.

The KGS (1) admits the following analytic solitary wave solution [19]:

$$\begin{cases} \psi(x - x_0, t, v) = \dfrac{3\sqrt{2}}{4\sqrt{1-v^2}} \operatorname{sech}^2 \dfrac{1}{2\sqrt{1-v^2}}(x - vt - x_0) \times \exp\left(\mathrm{i}\left(vx + \dfrac{1 - v^2 + v^4}{2(1-v^2)}t\right)\right), \\ \varphi(x - x_0, t, v) = \dfrac{3}{4(1-v^2)} \operatorname{sech}^2 \dfrac{1}{2\sqrt{1-v^2}}(x - vt - x_0), \end{cases} \tag{32}$$

where $|v| < 1$ is the propagating velocity of the solitary wave, and x_0 is the initial phase.

Table 1. Spatial accuracy for $m = 1$, $\tau = 0.000\,04$.

	$\text{Error}_{\|\psi\|}$		Order_{ψ}		Error_{φ}		Order_{φ}	
h	L_∞	L_2	L_∞	L_2	L_∞	L_2	L_∞	L_2
0.5	4.650×10^{-1}	1.529×10^{-2}	–	–	2.311×10^{-1}	1.123×10^{-3}	–	–
0.25	1.143×10^{-1}	2.643×10^{-3}	2.02	2.53	5.504×10^{-2}	1.205×10^{-3}	2.07	2.26
0.125	2.839×10^{-2}	4.636×10^{-4}	2.00	2.51	1.373×10^{-2}	2.105×10^{-4}	2.00	2.51
0.0625	7.080×10^{-3}	8.177×10^{-5}	2.00	2.50	3.428×10^{-3}	3.710×10^{-5}	2.00	2.50

Table 2. Spatial accuracy for $m = 2$, $\tau = 0.000\,04$.

	$\text{Error}_{\|\psi\|}$		Order_{ψ}		Error_{φ}		Order_{φ}	
h	L_∞	L_2	L_∞	L_2	L_∞	L_2	L_∞	L_2
1	6.697×10^{-1}	3.127×10^{-2}	–	–	5.048×10^{-1}	2.339×10^{-2}	–	–
0.5	4.219×10^{-2}	1.383×10^{-3}	3.99	4.49	2.093×10^{-2}	6.376×10^{-3}	3.91	4.44
0.25	2.786×10^{-3}	6.406×10^{-5}	3.96	4.46	1.388×10^{-3}	2.934×10^{-5}	4.25	4.81
0.125	1.765×10^{-4}	2.873×10^{-6}	3.98	4.47	8.825×10^{-5}	1.316×10^{-6}	3.98	4.47

Table 3. Spatial accuracy for $m = 3$, $\tau = 0.000\,04$.

	$\text{Error}_{\|\psi\|}$		Order_{ψ}		Error_{φ}		Order_{φ}	
h	L_∞	L_2	L_∞	L_2	L_∞	L_2	L_∞	L_2
1	3.307×10^{-1}	1.568×10^{-2}	–	–	2.630×10^{-1}	1.148×10^{-2}	–	–
0.5	6.575×10^{-3}	2.102×10^{-4}	5.65	6.22	3.182×10^{-3}	9.445×10^{-5}	6.36	6.22
0.25	1.203×10^{-4}	2.698×10^{-6}	5.77	6.28	5.820×10^{-5}	1.206×10^{-6}	5.77	6.29
0.125	1.668×10^{-6}	2.633×10^{-8}	6.17	6.67	9.378×10^{-7}	1.359×10^{-8}	5.95	6.47

4.1. Accuracy tests

In order to calculate the convergence ratio in space, we utilize the formulation

$$\text{order} \approx \frac{\ln(\|\text{error}(h_2)\|_\alpha / \|\text{error}(h_1)\|_\alpha)}{\ln(h_2/h_1)}, \tag{33}$$

where $\text{error}(h_k) = u(jh_k, t_n) - u_j^n$ indicates that the error is brought about by the spatial discretization with the step size h_k, and $\alpha = 2$ or $\alpha = \infty$. The calculating formula of convergence ratio in time has a similar formation to formula (33).

For convenience, we naturally take the initial conditions

$$\psi_0(x) = \psi(x - x_0, 0, v), \qquad \varphi_0(x) = \varphi(x - x_0, 0, v), \qquad \varphi_1(x) = \varphi_t(x - x_0, t, v)|_{t=0},$$

that is, they are obtained from the exact solution (32) as $t = 0$.

We take velocity $v = 0.5$ and initial phase $x_0 = -5$ in the subsection.

First, we test the spatial accuracy. We let the temporal step size τ be plenarily small, e.g., $\tau = 0.000\,04$, such that the discrete error from temporal discretization is negligible compared to that from space. We choose the spatial interval $[-20, 20]$, and compute the problem by symplectic approximation (13)–(14) with $m = 1, 2, 3$, up to $t = 20$. The errors, orders and spatial mesh sizes for $m = 1, 2, 3$ are listed in tables 1–3, respectively.

Table 4. Temporal accuracy for $m = 1, h = 0.031\,25$.

	$\text{Error}_{\|\psi\|}$		Order_{ψ}		Error_{φ}		Order_{φ}	
h	L_∞	L_2	L_∞	L_2	L_∞	L_2	L_∞	L_2
0.16	6.782×10^{-2}	4.583×10^{-4}	–	–	2.452×10^{-3}	1.492×10^{-5}	–	–
0.08	1.582×10^{-2}	1.067×10^{-4}	2.09	2.10	6.041×10^{-4}	6.041×10^{-6}	2.02	1.95

Table 5. Temporal accuracy for $m = 2, h = 0.125$.

	$\text{Error}_{\|\psi\|}$		Order_{ψ}		Error_{φ}		Order_{φ}	
h	L_∞	L_2	L_∞	L_2	L_∞	L_2	L_∞	L_2
0.04	4.394×10^{-3}	4.199×10^{-5}	–	–	1.979×10^{-4}	1.706×10^{-6}	–	–
0.02	1.091×10^{-3}	1.042×10^{-5}	2.00	2.00	4.590×10^{-5}	3.932×10^{-7}	2.10	2.11
0.01	2.648×10^{-4}	2.528×10^{-6}	2.04	2.04	7.961×10^{-6}	7.154×10^{-8}	2.52	2.45

Table 6. Temporal accuracy for $m = 3, h = 0.125$.

	$\text{Error}_{\|\psi\|}$		Order_{ψ}		Error_{φ}		Order_{φ}	
h	L_∞	L_2	L_∞	L_2	L_∞	L_2	L_∞	L_2
0.04	4.403×10^{-3}	5.952×10^{-5}	–	–	2.016×10^{-4}	2.468×10^{-6}	–	–
0.02	1.100×10^{-3}	1.487×10^{-5}	2.00	2.00	4.986×10^{-5}	6.094×10^{-7}	2.01	2.01
0.01	2.738×10^{-4}	3.700×10^{-6}	2.00	2.00	1.191×10^{-5}	1.443×10^{-7}	2.06	2.07

Next, we test the temporal accuracy. In order to do so, we make the spatial mesh size sufficiently small, such that the discrete error from spatial discretization is negligible compared to that from time. Choosing $h = 0.031\,25$ for $m = 1$, and $h = 0.125$ for $m = 2, 3$, we solve the problem with the approximation (13)–(14) till $t = 20$ on the spatial domain $[-20, 20]$. Tables 4–6 list the relationship among errors, orders and temporal step sizes for $m = 1, 2, 3$, respectively.

From tables 1–6, we can draw the following observations: approximation (13)–(14) are of $2m$th order accuracy in space, and of second-order accuracy in time.

4.2. Conservation law test and single soliton simulation

In the subsection, we examine the charge conservation law and residual of energy, as well as single soliton simulated by the symplectic approximation (13)–(14).

We choose the spatial interval $[-40, 40]$, and velocity $v = 0.5$, as well as initial phase $x_0 = -25$. The problem is simulated by the symplectic approximation (13)–(14) with $m = 1, 2, 3$ under different mesh divisions till $t = 100$. The mesh lengths are $\tau_1 = 0.2, h_1 = 0.5$; $\tau_2 = 0.1, h_2 = 0.25$. The error of charge and residual of energy are presented in figures 1 and 2, respectively, and figure 3 shows the soliton shapes of the neutron field $|\psi(x, t)|$ and neutral field $\varphi(x, t)$ with the mesh division $\tau_2 = 0.1, h_2 = 0.25$ at different time stages. Judged from figures 1–3, the error of charge is within the roundoff error. Although the energy is not conserved, its residual is very small during a long time, moreover, takes on quasi-periodic changes. Furthermore, soliton shapes are preserved very well during a long time in that the numerical solution and the exact solution are almost superposition.

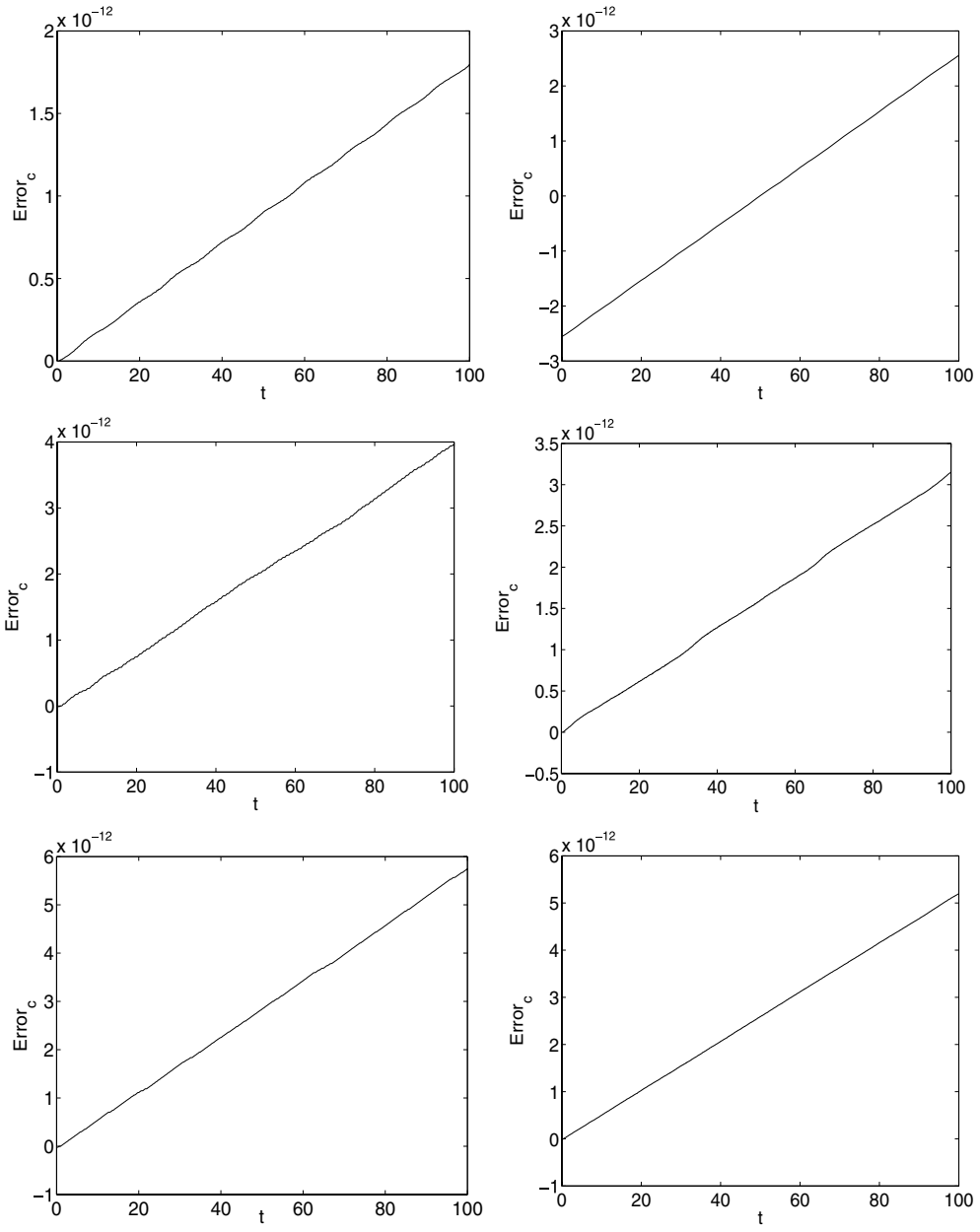

Figure 1. Error of charge: the first row: $m = 1$; the second row: $m = 2$; the third row: $m = 3$; the first line: $\tau = 0.2$, $h = 0.5$; the second line: $\tau = 0.1$, $h = 0.25$.

Remark 3. The problems including the above and the following problems, can be simulated over much longer time interval than what they have done, as long as the spatial domain is large enough. However, we cannot simulate them too long for the limitation of the length of spatial domains because of the size of memory.

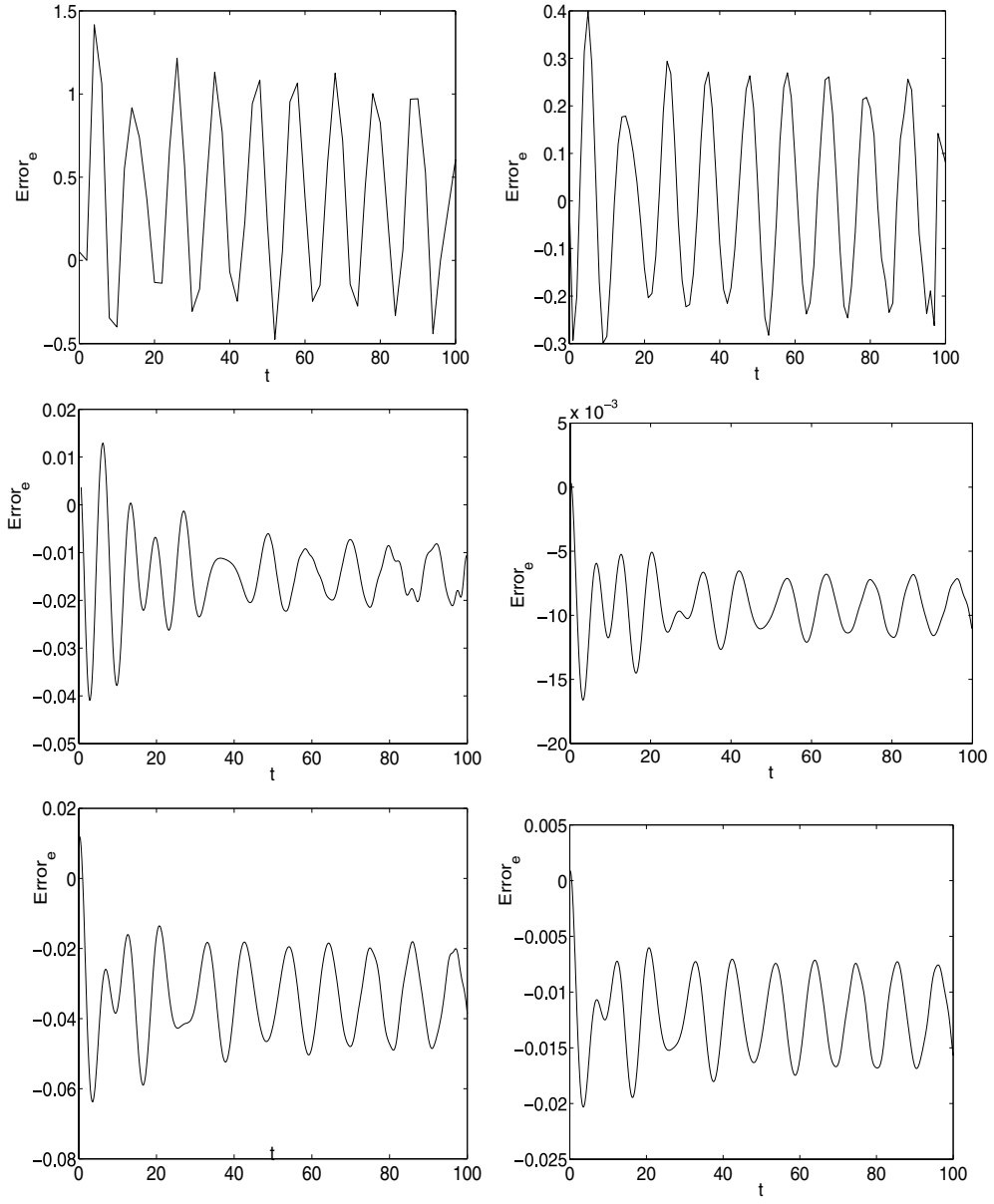

Figure 2. Residuals of energy: the first row: $m = 1$; the second row: $m = 2$; the third row: $m = 3$; the first line: $\tau = 0.2, h = 0.5$; the second line: $\tau = 0.1, h = 0.25$.

4.3. Plane-wave solution

In the subsection, we consider the plane-wave solution of the KGS with periodic boundary condition in the spatial interval $[0, \sqrt{2}\pi]$, that is,

$$\psi(0, t) = \psi(\sqrt{2}\pi, t), \qquad \varphi(0, t) = \varphi(\sqrt{2}\pi, t). \tag{34}$$

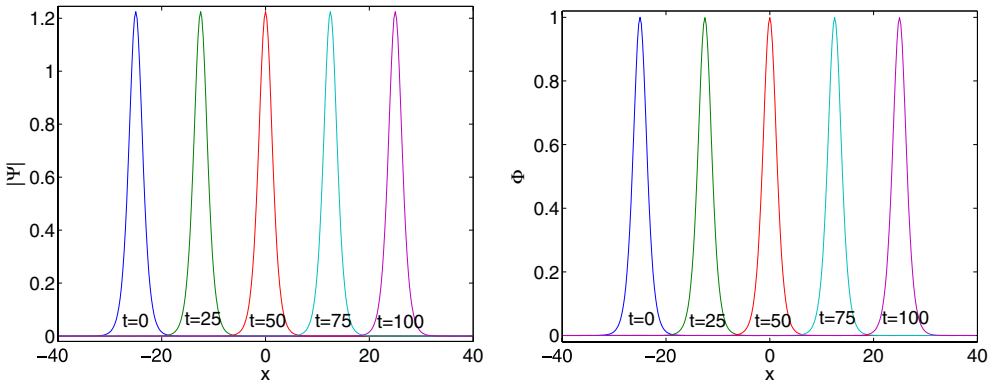

Figure 3. Soliton shape at different time: left, $|\psi(x,t)|$; right, $\varphi(x,t)$.

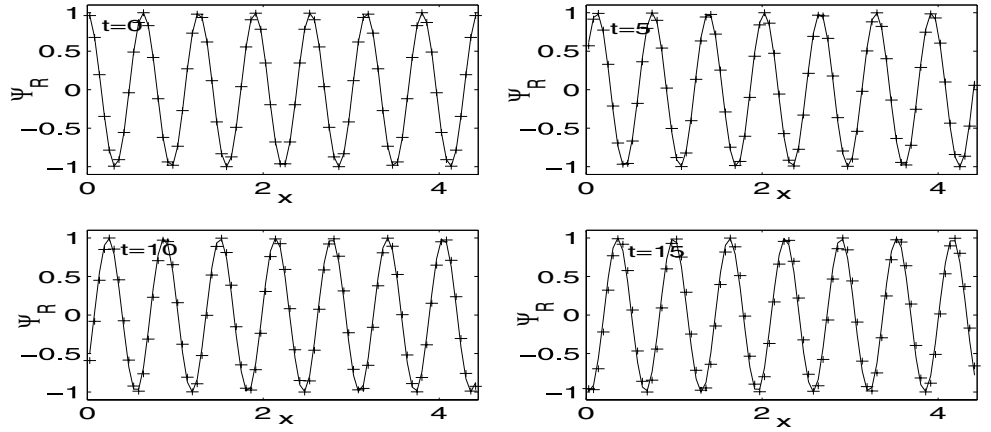

Figure 4. Plane-wave solution at different time of the real part of $\psi(x,t)$.

The initial conditions are taken as

$$\psi_0(x) = \mathrm{e}^{\mathrm{i}7\sqrt{2}x}, \qquad \varphi_0(x) = 1, \qquad \varphi_1(x) = 0. \tag{35}$$

Under the above initial-boundary conditions, the problem (1), (34), (35) admits the theoretical plane-wave solution

$$\begin{cases} \psi(x,t) = \mathrm{e}^{\mathrm{i}(7\sqrt{2}x - 48t)}, \\ \varphi(x,t) = 1. \end{cases} \tag{36}$$

To numerically simulate the problem, there is a little difference in dealing with the boundary conditions from the other problems in the section. The matrices B_{2m} should be the circulant matrices mentioned in section 2. We solve the problem by the symplectic approximation (13)–(14) with $m = 2$ under mesh step size $h = \frac{\sqrt{2}}{80}\pi$, $\tau = 0.001$ till $t = 15$. Figures 4, 5 and 6 compare the numerical results with the exact solution at different time stages. From these figures, we can see that the symplectic approximation (13)–(14) really simulates the original plane-wave solution from the beginning to the end.

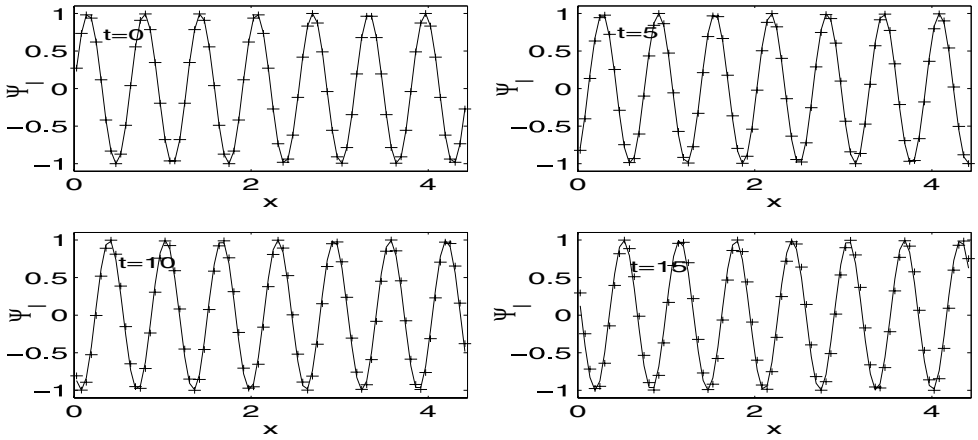

Figure 5. Plane-wave solution at different time of the imaginary part of $\psi(x, t)$.

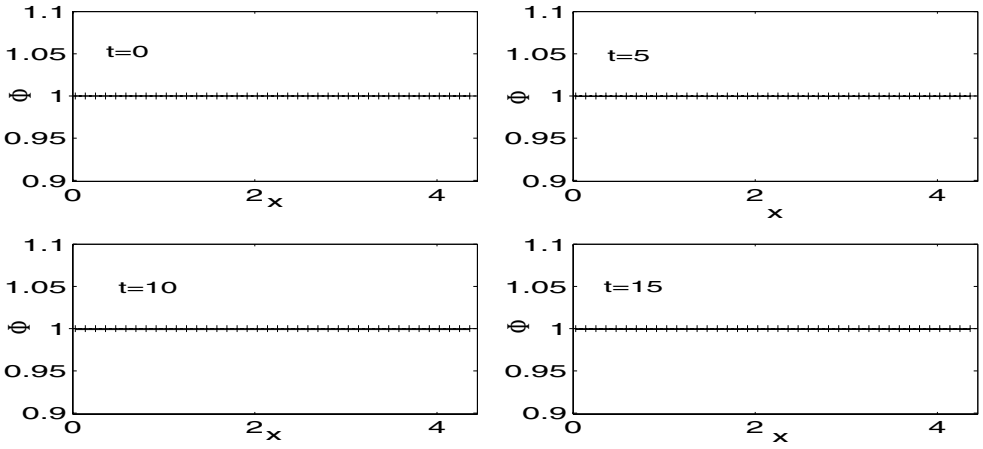

Figure 6. Plane-wave solution at different time of $\varphi(x, t)$.

In the following subsections, we turn our attention to the collision between two solitons, including symmetric and asymmetric soliton–soliton collision. For simplicity, we take the corresponding initial values as

$$\begin{cases} \psi(x) = \psi(x - p_1, 0, v_1) + \psi(x - p_2, 0, v_2), \\ \varphi(x) = \varphi(x - p_1, 0, v_1) + \varphi(x - p_2, 0, v_2), \\ \varphi_1(x) = \varphi_t(x - p_1, 0, v_1) + \varphi_t(x - p_2, 0, v_2), \end{cases} \tag{37}$$

where v_1, p_1 and v_2, p_2 are velocities and initial phases of the first and the second solitons, respectively, and $\psi(x, t, v)$ and $\varphi(x, t, v)$ are the exact solution (32).

4.4. Symmetric soliton–soliton collision

In what follows, we consider symmetric soliton–soliton collision, which can often be observed in quantum mechanics and fluid dynamics.

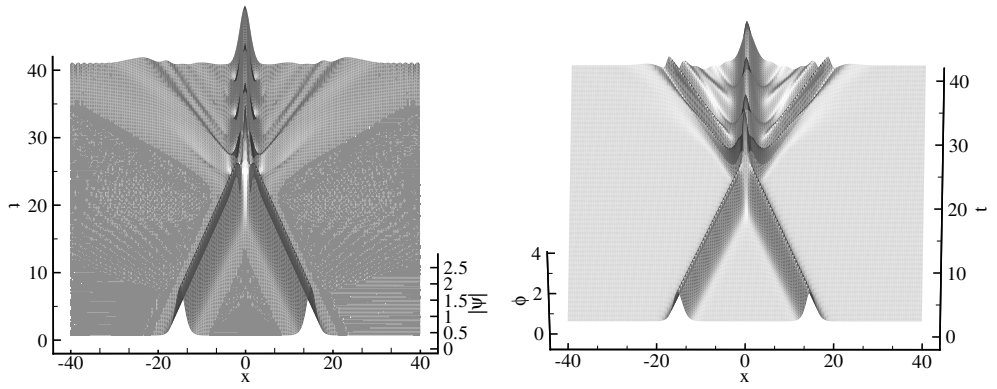

Figure 7. The symmetric collisions solitons: left, $\psi(x,t)$; right, $\varphi(x,t)$.

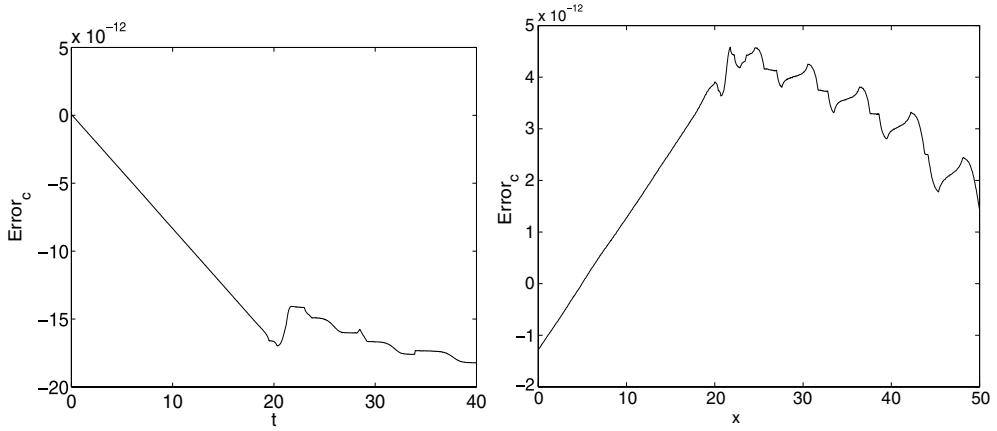

Figure 8. Error of charge: left, symmetric collision; right, asymmetric collision.

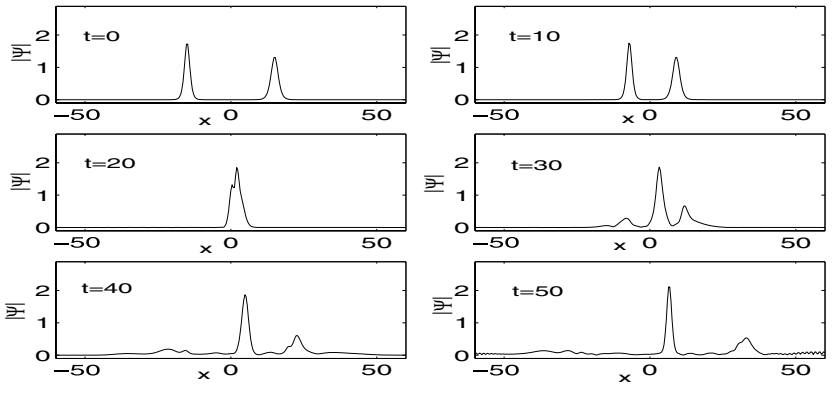

Figure 9. The asymmetric collisions solitons: neutron field $\psi(x,t)$.

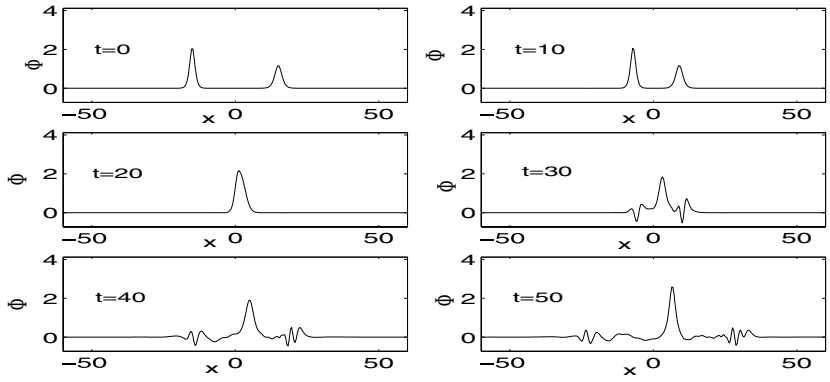

Figure 10. The asymmetric collisions solitons: neutral field $\varphi(x, t)$.

We choose velocities $v_1 = 0.7$, $v_2 = -0.7$ and initial phases $p_1 = -15$, $p_2 = 15$. The solution corresponding to the case is two solitons with the same velocities but in opposite directions and symmetrically distributing around the origin. The solitons are said to be symmetric solitons. We apply approximation (13)–(14) with $m = 2$ to solve the problem in the spatial interval $[-40, 40]$, as far as $t = 40$ under mesh division $\tau = 0.02, h = 0.2$. The evolution of the neutron field $|\psi(x, t)|$ and neutral field $\varphi(x, t)$ with temporal development are figured in figure 7. And the relationship between the error of charge and time is presented on the left side of figure 8. We can find that the two solitons keep their own shapes and velocities unchanged before collision, while result in fusion, and are accompanied by a series of emission of waves after interaction, and some new soliton-like waves are produced which are symmetrically distributed. Furthermore, the error of charge is within the roundoff error.

4.5. Asymmetric soliton–soliton collision

In the subsection, we go on considering the colliding phenomena between two head-on solitons which are asymmetric.

We take velocities $v_1 = 0.8$, $v_2 = -0.6$ and initial phases $p_1 = -15$, $p_2 = 15$, which describes two solitons propagating with both different velocities and different directions as well. The problem is considered in the space-time domain $(x, t) \in [-60, 60] \times [0, 50]$, and is simulated by the scheme (13)–(14) with $m = 2$ under the mesh division $h = 0.4$, $\tau = 0.05$. The 2D pictures of the waves for $|\psi(x, t)|$ and $\varphi(x, t)$ are shown in figures 9 and 10. And the error of charge is exhibited on the right side of figure 8. From the figures, we can discover that two solitons are merged into a larger one about $t = 20$, and some soliton-like waves brought out after collision, however, the collision is quite elastic. Above all, the charge is conserved exactly.

5. Conclusions and remarks

We have discussed a family of symplectic approximation for the KGS which is widely applied to describe the interaction between the complex neutron field and real neutral field in quantum mechanics. The following conclusions can be discovered from the above theoretical analysis and numerical examples.

The symplectic approximation can keep exactly the symplectic geometric structure of the original Hamiltonian system. They can simulate various solitons during a long period provided that the homogeneous or periodic boundary conditions are well satisfied all along. However, the solitary waves we consider in the numerical examples are almost hyperbolic sine wave. The spatial domain $[-L, L]$ must be adequately large for large time T to meet the homogeneous boundary conditions. Unfortunately, the spatial domain cannot be too large for the limitation of the size of memory and the spatial step size. The symplectic approximation we construct can preserve the charge exactly for the KGS. They cannot preserve the energy because the Hamiltonian function of the KGS is of degree 3. Fortunately, its residual is small, and takes on quasi-periodic fluctuation sometimes. They give an accurate plane-wave solution for the KGS. Moreover, the numerical solutions convergent to the exact solutions with $\mathcal{O}(\tau^2 + h^{2m})$. The symplectic approximation is efficient, accurate, unconditionally stable and can easily be generalized to 2D and 3D cases as well.

Acknowledgments

Linghua Kong is supported by the Doctor Foundation of Jiangxi Normal University (no 2057) and State Key Laboratory of Scientific and Engineering Computing, Chinese Academy of Sciences, Jialin Hong is supported by the Director Innovation Foundation of ICMSEC and AMSS, the Foundation of CAS, the NNSFC (no 19971089, no 10371128) and the Special Funds for Major State Basic Research Projects of China 2005CB321701. Ruxun Liu is supported by the NNSFC (10771138).

References

[1] Feng K 1985 On difference schemes and symplectic geometry *Proc. of the 1984 Beijing Symp. on Diff. geometry and Diff. equations* ed K Feng (Beijing: Science Press) pp 42–58
[2] Channel P J and Scovel C 1990 Symplectic integration of Hamiltonian systems *Nonlinearity* **3** 231–59
[3] Qin M Z and Zhu W J 1993 Construction of symplectic schemes for wave equations via hyperbolic functions $\sinh(x)$, $\cosh(x)$, and $\tanh(x)$ *Comput. Math. Appl.* **26** 1–11
[4] Liu X S, Qi Y Y, He J F and Ding P Z 2007 Recent progress in symplectic algorithms for use in quantum systems *Commun. Comput. Phys.* **2** 1–53
[5] Mclachlan R 1994 Symplectic integration of Hamiltonian wave equations *Numer. Math.* **66** 465–92
[6] Budd C J and Piggott M D 2003 Geometric integration and its application *Handbook Numer. Anal.* vol XI (Amsterdam: North-Holland) pp 35–139
[7] Sanz-Serna J M and Calvo M P 1994 *Numerical Hamiltonian Problems* (London: Chapman and Hall)
[8] Tang Y F, Pérez-Garcia V M and Vázquez L 1997 Symplectic methods for the Ablowitz-ladik model *Appl. Math. Comput.* **82** 17–38
[9] Duncan D B 1996 Symplectic finite difference approximation of the nonlinear Klein-Gordon equation *SIAM J. Numer. Anal.* **34** 1742–60
[10] Cano B 2006 Conserved quantities of some Hamiltonian wave equations after full discretization *Numer. Math.* **103** 197–223
[11] Morton K W and Mayers D F 2005 *Numerical Solution of Partial Differential Equations* (Cambridge: Cambridge University Press)
[12] Fukuda I and Tsutsumi M 1975 On the Yukawa coupled Klein-Gordon-Schrödinger equations in R^3 *Proc. Japan Acad.* **51** 402–5
[13] Fukuda I and Tsutsumi M 1978 On coupled Klein-Gordon-Schrödinger equations II *J. Math. Anal. Appl.* **66** 358–78
[14] Guo B L and Miao C X 1995 Asymptotic behavior of coupled Klein-Gordon-Schrödinger equations *Sci. China Ser.* A **25** 705–14
[15] Guo B L and Li Y S 1997 Attractor for dissipative Klein-Gordon-Schrödinger equations in R^3 *J. Diff. Eqns.* **136** 356–77

[16] Hayashi N and von Wahl W 1987 On the global strong solutions of coupled Klein-Gordon-Schrödinger equations *J. Math. Soc. Japan* **39** 489–97
[17] Ohta M 1996 Stability of stationary states for coupled Klein-Gordon-Schrödinger equations *Nonlinear Anal.* **27** 455–61
[18] Hioe F T 2003 Periodic solitary waves for two coupled nonlinear Klein-Gordon and Schrödinger equations *J. Phys. A: Math. Gen.* **36** 7307–30
[19] Wang M L and Zhou Y B 2003 The periodic wave solutions for the coupled Klein-Gordon-Schrödinger equations *Phys. Lett.* A **318** 84–92
[20] Darwish A and Fan E G 2004 A series of new explicit exact solutions for the coupled Klein-Gordon-Schrödinger equations *Chaos Solitons Fractals* **20** 609–17
[21] Zhang L M 2005 Convergence of a conservative difference scheme for a class of Klein-Gordon-Schrödinger equations in one space dimension *Appl. Math. Comput.* **163** 343–55
[22] Zhang L M and Chang Q S 2000 Convergence and stability of a conservative finite difference scheme for a class of equation system in interaction of complex Schrödinger field and real Klein-gordon field *Numer. Math. J. Chin. Univ.* **22** 362–70
[23] Xiang X M 2004 The long time behavior of spectral approximate for Klein-Gordon-Schrödinger equations *J. Comput. Math.* **22** 89–100
[24] Kong L H, Liu R X and Xu Z L 2006 Numerical simulation of interaction between Schrödinger field and Klein-gordon field by multisymplectic method *Appl. Math. Comput.* **181** 342–50
[25] Kong L H, Hong J L, Liu Ruxun and Jiang S S Efficient multisymplectic Fourier pseudo-spectral scheme for Klein-Gordon-Schrödinger equations submitted
[26] Hong J L, Jiang S S and Li C Error analysis of some multisymplectic schemes for Klein-Gordon-Schrödinger equations http://icmsec.cc.ac.cn/06research_report/0612.pdf (in preprint)
[27] Bao W Z and Yang L 2007 Efficient and accurate numerical methods for the Klein-Gordon-Schrödinger equations *J. Comput. Phys.* **225** 1863–93
[28] Zhou Y L 1990 *Application of Discrete Functional Analysis to the Finite Difference Method* (Hong Kong: International academic publishers)